

Surgical Aggregation: A Federated Learning Framework for Harmonizing Distributed Datasets with Diverse Tasks

Pranav Kulkarni¹

PKULKARNI@SOM.UMARYLAND.EDU

Adway Kanhere^{1,2}

AKANHERE@SOM.UMARYLAND.EDU

Paul H. Yi¹

PYI@SOM.UMARYLAND.EDU

Vishwa S. Parekh¹

VPAREKH@SOM.UMARYLAND.EDU

¹ *University of Maryland Medical Intelligent Imaging (UM2i) Center*

University of Maryland School of Medicine, Baltimore, MD 21201

² *Department of Biomedical Engineering, Johns Hopkins University, Baltimore, MD 21218*

Editors: Under Review for MIDL 2023

Abstract

Many large-scale chest x-ray datasets have been curated for the detection of abnormalities using deep learning, with the potential to provide substantial benefits across many clinical applications. However, these datasets focus on detecting a subset of disease labels that could be present, thus limiting their clinical utility. Furthermore, the distributed nature of these datasets, along with data sharing regulations, makes it difficult to share and create a complete representation of disease labels. To that end, we propose surgical aggregation, a federated learning framework for aggregating and harmonizing knowledge from distributed datasets with different disease labels into a ‘global’ deep learning model. We utilized surgical aggregation to harmonize the NIH (14 labels) and CheXpert (13 labels) datasets into a global model with the ability to predict all 20 unique disease labels and compared it to the performance of ‘baseline’ models trained individually on both datasets. We observed that the global model resulted in excellent performance across held-out test sets from both datasets with an average AUROC of 0.75 and 0.74 respectively when compared to the baseline average AUROC of 0.81 and 0.71. On the MIMIC external test set, we observed that the global model had better generalizability with average AUROC of 0.80, compared to the average AUROC of 0.74 and 0.76 respectively for the baseline models. Our results show that surgical aggregation has the potential to develop clinically useful deep learning models by aggregating knowledge from distributed datasets with diverse tasks – a step forward towards bridging the gap from bench to bedside.

Keywords: Deep learning, federated learning, surgical aggregation, data harmonization, chest x-ray, classification.

1. Introduction

Chest X-Ray (CXR) is the most commonly ordered medical imaging study globally and is critical for screening many life threatening conditions. As a result, many large-scale public CXR datasets have been released through curation of Wang et al. (2017), Irvin et al. (2019), Johnson et al. (2019), and Nguyen et al. (2022) for the purpose of training clinically-useful deep learning models for detection of diseases in the thorax. These, in turn, have resulted in numerous narrowly-focused ‘toy’ datasets as part of data science competitions hosted on platforms like Kaggle resulting in expert-level performance for single disease diagnoses.

The release of these datasets has spearheaded the utility of deep learning in medical imaging by providing expert-level detection of diseases using CXRs. Unfortunately, due to the nature of curating large-scale datasets, these datasets are often distributed and focus on detecting different disease labels. Furthermore, due to the patient data privacy regulations, it is difficult to share large-scale private datasets across multiple institutions to create a complete representation of disease labels. As a result, these datasets can be considered ‘incomplete’ since information about labels present in one dataset may not be available in another. For example, the NIH Chest X-Ray 14 (‘NIH’) (Wang et al., 2017) dataset consists of 14 labels while the CheXpert and MIMIC-CXR-JPG datasets Irvin et al. (2019), Johnson et al. (2019) consist of 13 labels (excluding the label for normal). Despite having 7 labels in common (Fig. 1) all three datasets are distributed and incomplete due to differences in disease labels. As a result, naïvely training a deep learning model on all three datasets, without harmonizing them first, could lead to incomplete and inaccurate representation of the distribution.

NIH	CheXpert/MIMIC-CXR
Atelectasis	Atelectasis
Cardiomegaly	Cardiomegaly
Consolidation	Consolidation
Edema	Edema
Effusion	Effusion
Emphysema	Enlarged Cardiom.
Fibrosis	Fracture
Hernia	Lung Lesion
Infiltration	Lung Opacity
Mass	Pleural Other
Nodule	Pneumonia
Pleural_Thickening	Pneumothorax
Pneumonia	Support Devices
Pneumothorax	

Figure 1: Comparison of disease and finding labels between NIH and CheXpert datasets. Overlapping labels highlighted in blue.

This fact is easily observed with smaller-scale toy datasets. While useful from a data science competition standpoint, they have limited clinical utility because of their narrow focus on one single diagnostic task. For example, the two Kaggle CXR competitions hosted by RSNA and SIIM have focused on diagnosis of a single disease – pneumonia and pneumothorax (Yi et al., 2021). Although impressive results have resulted from these competitions, their utility is limited given the dozens of diagnoses that could present in real-world clinical practice and the possibility of a patient being diagnosed with both pneumonia and pneumothorax. Since both datasets are subsets of the larger NIH dataset, we can observe that out of the 2,495 patients diagnosed with either pneumonia or pneumothorax, 185 patients were diagnosed with both (Appendix Fig. 3). Thus, making both toy datasets, and any other derivatives of the NIH dataset, distributed and incomplete.

Therefore, a method to harmonize these CXR datasets to train a clinically-useful model could revolutionize how distributed and incomplete datasets with different disease labels can be leveraged in aggregate for development of clinically-relevant deep learning models. To that end, we propose surgical aggregation, a federated learning framework for aggregating knowledge from spatially distributed datasets with incomplete and different disease annotations into a ‘global’ deep learning model. In this work, we demonstrate the potential for surgical aggregation to develop clinically useful deep learning models by aggregating knowledge from distributed datasets with diverse tasks.

2. Prior Research

Federated learning (FL) is a collaborative machine learning technique that approaches the problem of training a global model on non-iid data from a multi-domain and multi-task perspective. By using a decentralized and distributed approach, consisting of a central server and nodes, a global model can be trained to generalize distributed tasks with non-iid labels. In the realm of medical imaging, FL has enabled training of large-scale global deep learning models using homogenous data spread across multiple institutions without sharing sensitive patient data (Rieke et al., 2020; Chowdhury et al., 2022). However, majority of the datasets being curated across the world are heterogenous and focus on similar but different tasks. As a result, in the context of domain adaption, tackling non-iid data with domain shift is crucial. Consequently, different strategies and heuristics have been proposed in the literature for aggregating knowledge from heterogeneous datasets to tackle domain shift (Li et al., 2021; Gong et al., 2021, 2022; Kulkarni et al., 2022; Arasteh et al., 2022). However, this is a recent and relatively unexplored field in deep learning for medical imaging.

Knowledge distillation has emerged as a popular technique across multiple domains for aggregating knowledge from heterogeneous datasets to tackle domain shift (Li and Wang, 2019; Li et al., 2021; Chang et al., 2019; Gong et al., 2021, 2022). Gong et al. (2022) explored an ensemble attention distillation based FL approach to harmonize the NIH and CheXpert datasets, demonstrating the ability to train a global model with 14 disease labels, with 12 from CheXpert and 8 from the NIH dataset. However, the proposed approach required a separate external dataset and worked only in a multi-class scenario i.e. a patient could not be diagnosed with more than one disease, making it practically challenging and not clinically-relevant. Alternatively, a different approach, proposed recently, involved aggregating only the network backbone during FL training (Arasteh et al., 2022). However, this approach involved further training of the local models post FL aggregation resulting in different local models optimized for their respective tasks as opposed to a single multi-task global model.

In this work, we propose surgical aggregation wherein the server surgically aggregates relevant knowledge coming in from each node to effectively learn different tasks across distributed and heterogeneous datasets. Our proposed technique does not require any additional external dataset for training, is developed to handle scenarios where contributing datasets contain different, overlapping, and incomplete labels, and can be implemented in a local as well as decentralized setup. We evaluated surgical aggregation on synthetic toy datasets created from the NIH dataset as well as on aggregating knowledge from NIH and CheXpert datasets into a ‘global’ model.

3. Methods

3.1. Surgical Aggregation

We developed surgical aggregation as a model and task-agnostic framework for ‘surgically’, i.e. selectively, aggregating weights corresponding to a certain diagnostic task during the aggregation step of each FL round. Let’s consider K datasets with L_1, L_2, \dots, L_K diseases labels, with or without overlapping labels. By utilizing surgical aggregation, the global model can predict the presence of all $\bigcup_{i=1}^K L_i$ unique disease labels present across all K datasets, as visualized in Fig. 2.

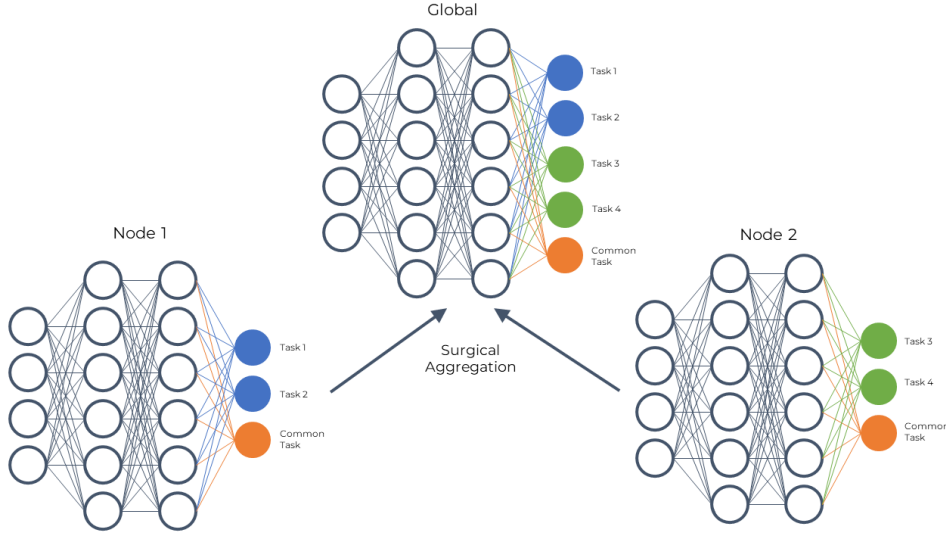


Figure 2: An overview of the surgical aggregation framework.

We initialized our FL setup as a multi-task and multi-label deep neural network composed of a central server and two nodes. The model consists of two distinct blocks - a representation block and a task block. In such a setup, the representation block learns a generalized global representation of the data using extracted feature semantics while the task block learns to interpret this representation and predict the presence of abnormalities. During training, the weights corresponding to the representation block are always aggregated and redistributed by the central server back to the nodes, thereby developing a generalized representation for different tasks in the representation block. In contrast, the weights from each task block are surgically aggregated to aggregate task-related knowledge from each node into a global task block. If a disease label is shared across one or more nodes, the weight and bias applied to the input of the neuron corresponding to that label in the task block are aggregated using a strategy (for eg., FedAvg). However, if a disease label is unique to the node, the weights remain unchanged. This enables the selective aggregation of the weights applied to the input of the task block and enables the global model to construct a task block that is an aggregation of the knowledge learned for all disease labels from all nodes. The surgical aggregation framework is described in detail in Algorithm 1.

In our implementation, we utilized a DenseNet121 model architecture, initialized with ImageNet weights. Prior to surgical aggregation, classification heads of all local models were warmed-up using transfer learning. For weight aggregation for both representation and task blocks, we implemented FedAvg, as described in McMahan and more (2017). The surgical aggregation was applied to the final fully-connected Dense classification layer.

3.2. Datasets

3.2.1. NIH CHEST X-RAY 14

The NIH dataset, curated by Wang et al. (2017), consists of 14 disease labels (Fig. 1) with $N=112,120$ frontal-view CXRs from $M=30,805$ patients. We randomly divided the dataset

Algorithm 1: Surgical Aggregation

Input: K clients indexed by k , with local labels L_k and final Dense layer weights w_k ;

Aggregation strategy F ;

Output: w_g , the final Dense layer weights for the global model

```

 $L_g \leftarrow \bigcup_{k=1}^K L_k$ 
for  $i \leftarrow 1$  to  $\text{length}(L_g)$  do
     $w_{agg} \leftarrow []$ 
    for  $k \leftarrow 1$  to  $K$  do
        if  $L_g[i]$  in  $L_k$  then
            append  $w_k$  to  $w_{agg}$ 
        end
    end
     $w_g[:, i] \leftarrow F(w_{agg})$ 
end

```

into training (70%, $N=78,571$, $M=21,563$), validation (10%, $N=11,219$, $M=3,080$), and testing (20%, $N=22,330$, $M=6,162$) splits while ensuring no patient appears in more than one split.

3.2.2. CHEXPERT

The Stanford CheXpert dataset, curated by Irvin et al. (2019), consists of 13 disease labels (Fig. 1) and an additional label for ‘normal’ with $N=224,316$ CXRs from $M=65,240$ patients. To handle uncertain labels in the dataset, we chose the U-Zeros approach i.e. treating all uncertain labels as negatives. We randomly divided the dataset into training (70%, $N=155,470$, $M=45,178$), validation (10%, $N=22,736$, $M=6,454$), and testing (20%, $N=45,208$, $M=12,908$) splits while ensuring no patient appears in more than one split.

3.2.3. MIMIC-CXR-JPG

To evaluate the generalizability of our methods, we utilized the MIMIC-CXR-JPG dataset, curated by Johnson et al. (2019) as our external test set. Similar to the CheXpert dataset, the MIMIC dataset consists of 13 disease labels (Fig. 1) and an additional label for ‘normal’ with $N=377,110$ CXRs from 65,379 patients. To handle uncertain labels in the dataset, we chose the U-Zeros approach i.e. treating all uncertain labels as negatives.

3.3. Experimental Setup

We conducted three preliminary experiments using toy datasets sampled from the NIH dataset, with overlapping and disjoint disease labels, followed by an experiment evaluating surgical aggregation using non-iid data with domain shift and distributed labels. For each experiment, patients diagnosed with at least one positive finding were equally distributed with healthy patients in each synthetically generated dataset to prevent patient overlap.

In the first experiment, we divided the NIH training (and validation) data into two toy datasets. The disease labels in the first and second toy datasets were randomly pruned to 11 and 7 labels, respectively, with 4 overlapping labels. Distribution of labels is highlighted

in Appendix Table 3. Similarly, the second experiment was set up by randomly pruning the disease labels to create two disjoint distributed and incomplete toy datasets with 7 labels each. Distribution of labels is highlighted in Appendix Table 4. In the third experiment, we randomly pruned all but one disease label from each patient to create 14 toy dataset nodes with one distinct label each. The surgically aggregated global model for each of these experiments would result in a model that can predict all 14 disease labels present in the NIH dataset. This enabled us to evaluate the framework on the known global ground truth for the held-out internal test set in an environment with non-iid data. We compared the performance of global models to a baseline model trained using complete data on the held-out internal test set. Additionally, we trained a model for each of these experiments without utilizing surgical aggregation and naïvely centralizing all incomplete toy datasets to a local location. This would allow us to establish an upper and lower bound for the expected performance of the surgically aggregated global models.

For the final experiment, we evaluated surgical aggregation in the context of domain adaption, using non-iid data with domain shift, and trained a global model that harmonizes the NIH and CheXpert datasets. In addition, we used differential learning rates at each local node to address domain shift. Our surgically aggregated global model would result in a model that can predict all 20 unique disease labels present across both datasets, with 7 overlapping labels (Fig. 1). Additionally, we trained baseline models individually on both datasets as well as two naïve approaches without utilizing surgical aggregation. In the first approach, we trained a model by naïvely concatenating both datasets in a local and centralized setup. In the second approach, we trained a global model using FedAvg without the added complexity of surgical aggregation in a 2-node FL setup. We initialized both nodes with all 20 labels and computed partial local losses using only the observed tasks in each node. Using held-out internal testing sets from both datasets, we compared the performance of all 4 baseline models and the surgically aggregated global model. We calculated model metrics across the observed disease labels in the test set as well as the 7 common labels found in both datasets. Finally, we evaluated the generalizability and performance of the surgically aggregated and baseline models on the external MIMIC test set across all 13 CheXpert disease labels and the 7 common labels (Fig. 1) found in all three datasets.

As model metrics, we used binary cross-entropy loss (BCE) and the average area under receiver operating characteristic curve (AUROC) score. In a multi-label scenario, the AUROC score is defined as the mean AUROC score across all disease labels. The disease-level AUROC scores between the surgically aggregated global models and baseline models were compared using bootstrapping and two-tailed paired t-test. For all experiments, 95% CI for AUROC scores is provided and statistical significance was defined as $p < 0.05$.

4. Results

In both two-node preliminary experiments using toy datasets sampled from the NIH dataset, we observed excellent overall performance in diagnosing all 14 disease labels on the held-out internal testing set. The average AUROC for both the surgical aggregation global model trained on toy datasets with overlapping disease labels as well as the baseline model trained on complete data was 0.81 ($p = 0.12$). In comparison, the surgical aggregation

global model trained on toy datasets with disjoint labels resulted in an average AUROC of 0.80 ($p < 0.001$), as detailed in Table 1. The complete disease-level AUROC scores for both experiments are detailed in Appendix B. However, there was a significant drop in performance of the fourteen-node surgical aggregation model for the third preliminary experiment with an average AUROC of 0.71 ($p < 0.001$).

Table 1: Model metrics on held-out NIH test set across all 14 disease labels for toy datasets with (a) overlapping disease labels and (b) disjoint disease labels.

(a)			(b)		
Model	Loss	AUROC	Model	Loss	AUROC
Baseline	0.15	0.81 (0.81, 0.82)	Baseline	0.15	0.81 (0.81, 0.82)
Naïve	0.16	0.79 (0.78, 0.79)	Naïve	0.17	0.79 (0.78, 0.79)
Surgical Aggregation	0.15	0.81 (0.81, 0.82)	Surgical Aggregation	0.15	0.80 (0.80, 0.81)

When evaluating the performance of utilizing surgical aggregation to harmonize NIH and CheXpert datasets, we observed excellent overall performance when compared to the baseline models across held-out internal test sets from both datasets. Despite observing a significant drop in performance on the NIH test set ($p < 0.001$), our performance on the CheXpert test set improved significantly ($p < 0.001$). We observed a similar result when the 7 common labels were considered – the global model outperformed on the CheXpert dataset while underperforming on the NIH dataset when compared to all baseline models. However, when all observed labels were considered, the surgically aggregated global model outperformed all naïve approaches. On the MIMIC external test set, we observed similar results with the global model outperforming all baseline and naïve approaches ($p < 0.001$). The results are detailed in Table 2. Additional results on the CheXpert validation set are detailed in Appendix D.

5. Discussion

Although the release of large-scale CXR datasets has spearheaded the utility of deep learning models, the distributed nature of these datasets have limited their clinical utility. Our results demonstrate the utility of surgical aggregation in harmonizing and aggregating knowledge from heterogeneous, distributed, and incomplete large-scale CXR datasets. Furthermore, our results suggest that the surgically aggregated global model, not only tackles domain shift with non-iid data, but also results in a more generalizable model. In our preliminary experiments, we observed that the naïvely trained models performed similarly to both the baseline and surgically aggregated global models. We believe this is due to the lack of domain shift since both toy datasets were sampled from the same NIH dataset distribution.

In the context of domain adaption with non-iid data, we observed that all naïve approaches performed significantly worse when all observed disease labels were considered. While the performance of these naïve approaches on the 7 common labels was on par (or even better in one case) when compared to the surgically aggregated global model, these approaches fell short on disease labels that were not shared between the NIH and CheXpert

Table 2: Model metrics on held-out NIH and CheXpert test sets and external MIMIC test set across (a) the 7 common labels (Fig. 1) and (b) all labels.

(a)

Model	NIH		CheXpert		MIMIC-CXR	
	Loss	AUROC	Loss	AUROC	Loss	AUROC
NIH Baseline	0.15	0.83 (0.83, 0.84)	0.73	0.68 (0.67, 0.68)	0.37	0.74 (0.74, 0.74)
CheXpert Baseline	0.22	0.77 (0.77, 0.78)	0.44	0.74 (0.73, 0.74)	0.31	0.76 (0.76, 0.76)
Naïve	0.22	0.78 (0.77, 0.79)	0.44	0.73 (0.73, 0.74)	0.31	0.76 (0.76, 0.77)
Naïve FedAvg	0.18	0.83 (0.83, 0.84)	0.44	0.74 (0.74, 0.75)	0.28	0.78 (0.77, 0.78)
Surgical Aggregation	0.18	0.77 (0.76, 0.78)	0.43	0.76 (0.76, 0.77)	0.27	0.80 (0.80, 0.80)

(b)

Model	NIH		CheXpert		MIMIC-CXR	
	Loss	AUROC	Loss	AUROC	Loss	AUROC
NIH Baseline	0.15	0.81 (0.81, 0.82)	-	-	-	-
CheXpert Baseline	-	-	0.39	0.71 (0.71, 0.72)	0.28	0.69 (0.69, 0.69)
Naïve	0.28	0.67 (0.65, 0.68)	0.39	0.70 (0.70, 71)	0.28	0.71 (0.70, 0.71)
Naïve FedAvg	0.23	0.68 (0.67, 0.69)	0.44	0.69 (0.68, 0.69)	0.27	0.71 (0.71, 0.72)
Surgical Aggregation	0.17	0.75 (0.74, 0.76)	0.39	0.74 (0.73, 0.75)	0.25	0.74 (0.74, 0.74)

datasets. Our results suggest that, unlike the naïve approaches, surgical aggregation has the ability to learn a generalized distribution and potentially learn intrinsic relationships between similar but different tasks that warrants future research (Appendix E) and could justify the better generalizability of the surgically aggregated global model.

Our study has certain shortcomings, especially related to the scalability of surgical aggregation (Appendix C) as well as the significant impact on model performance. Due to the heterogeneous nature of these datasets, we observed that easy-to-learn tasks overfit early in the training process and poison the distribution learned by the representation block. Li et al. (2021) suggest utilizing batch normalization layers to tackle domain shift with non-iid data. Additionally, Li et al. (2019) conclude that the learning rate must decay in individual nodes to ensure convergence with non-iid data. For future work, We intend to explore these solutions on a larger-scale experiment and address shortcomings in our work.

Despite these shortcomings, our work demonstrates how large-scale CXR datasets can be leveraged in aggregate to train clinically-useful global models through data harmonization. We believe our work will open new avenues for the development of newer aggregation and convergence strategies and further research into the field of data harmonization – a step forward towards bridging the gap from bench to bedside.

References

Soroosh Tayebi Arasteh, Peter Isfort, Marwin Saehn, Gustav Mueller-Franzes, Firas Khader, Jakob Nikolas Kather, Christiane Kuhl, Sven Nebelung, and Daniel Truhn. Collaborative

- training of medical artificial intelligence models with non-uniform labels. *arXiv preprint arXiv:2211.13606*, 2022.
- Hongyan Chang, Virat Shejwalkar, Reza Shokri, and Amir Houmansadr. Cronus: Robust and heterogeneous collaborative learning with black-box knowledge transfer. *arXiv preprint arXiv:1912.11279*, 2019.
- Alexander Chowdhury, Hasan Kassem, Nicolas Padoy, Renato Umeton, and Alexandros Karargyris. A review of medical federated learning: Applications in oncology and cancer research. In *International MICCAI Brainlesion Workshop*, pages 3–24. Springer, 2022.
- Xuan Gong, Abhishek Sharma, Srikrishna Karanam, Ziyang Wu, Terrence Chen, David Doermann, and Arun Innanje. Ensemble attention distillation for privacy-preserving federated learning. In *Proceedings of the IEEE/CVF International Conference on Computer Vision*, pages 15076–15086, 2021.
- Xuan Gong, Liangchen Song, Rishi Vedula, Abhishek Sharma, Meng Zheng, Benjamin Planche, Arun Innanje, Terrence Chen, Junsong Yuan, David Doermann, et al. Federated learning with privacy-preserving ensemble attention distillation. *IEEE Transactions on Medical Imaging*, 2022.
- Jeremy Irvin, Pranav Rajpurkar, Michael Ko, Yifan Yu, Silvana Ciurea-Ilcus, Chris Chute, Henrik Marklund, Behzad Haghgoo, Robyn Ball, Katie Shpanskaya, et al. Chexpert: A large chest radiograph dataset with uncertainty labels and expert comparison. In *Proceedings of the AAAI conference on artificial intelligence*, volume 33, pages 590–597, 2019.
- Alistair EW Johnson, Tom J Pollard, Nathaniel R Greenbaum, Matthew P Lungren, Chihying Deng, Yifan Peng, Zhiyong Lu, Roger G Mark, Seth J Berkowitz, and Steven Horng. Mimic-cxr-jpg, a large publicly available database of labeled chest radiographs. *arXiv preprint arXiv:1901.07042*, 2019.
- Pranav Kulkarni, Adway Kanhere, Paul H Yi, and Vishwa S Parekh. From competition to collaboration: Making toy datasets on kaggle clinically useful for chest x-ray diagnosis using federated learning. *arXiv preprint arXiv:2211.06212*, 2022.
- Daliang Li and Junpu Wang. Fedmd: Heterogeneous federated learning via model distillation. *arXiv preprint arXiv:1910.03581*, 2019.
- Xiang Li, Kaixuan Huang, Wenhao Yang, Shusen Wang, and Zhihua Zhang. On the convergence of fedavg on non-iid data. *arXiv preprint arXiv:1907.02189*, 2019.
- Xiaoxiao Li, Meirui Jiang, Xiaofei Zhang, Michael Kamp, and Qi Dou. Fedbn: Federated learning on non-iid features via local batch normalization. *arXiv preprint arXiv:2102.07623*, 2021.
- Brendan McMahan and more. Communication-Efficient Learning of Deep Networks from Decentralized Data. In *Proceedings of the 20th International Conference on Artificial Intelligence and Statistics*, volume 54 of *Proceedings of Machine Learning Research*, pages 1273–1282. PMLR, 20–22 Apr 2017.

- Ha Q Nguyen, Khanh Lam, Linh T Le, Hieu H Pham, Dat Q Tran, Dung B Nguyen, Dung D Le, Chi M Pham, Hang TT Tong, Diep H Dinh, et al. Vindr-cxr: An open dataset of chest x-rays with radiologist’s annotations. *Scientific Data*, 9(1):1–7, 2022.
- Nicola Rieke, Jonny Hancox, Wenqi Li, Fausto Milletari, Holger R Roth, Shadi Albarqouni, Spyridon Bakas, Mathieu N Galtier, Bennett A Landman, Klaus Maier-Hein, et al. The future of digital health with federated learning. *NPJ digital medicine*, 3(1):1–7, 2020.
- Xiaosong Wang, Yifan Peng, Le Lu, Zhiyong Lu, Mohammadhadi Bagheri, and Ronald M Summers. Chestx-ray8: Hospital-scale chest x-ray database and benchmarks on weakly-supervised classification and localization of common thorax diseases. In *Proceedings of the IEEE conference on computer vision and pattern recognition*, pages 2097–2106, 2017.
- Paul H Yi, Tae K Kim, E Siegel, and Yahyavi-Firouz-Abadi N. Demographic reporting in publicly available chest radiograph data sets: Opportunities for mitigating sex and racial disparities in deep learning models. *Journal of the American College of Radiology*, 19(1 Pt B):192–200, 2021.

Appendix A. Disease Label Overlap in Diagnosed Patients

The co-occurrence matrix of disease labels, visualized in Appendix Fig. 3, for all diagnosed patients from the NIH dataset demonstrates the overlap of every disease label in the dataset with another label for every patient who is diagnosed. As a result, any derivative of the NIH dataset focusing on a single diagnostic task is inherently incomplete. Thus, data harmonization is crucial in leveraging multiple datasets in aggregate to train clinically-useful deep learnign models. The co-occurrence matrix was calculated by first determining the positive disease labels for each patient across all available studies and then determining the number of patients that have been diagnosed for each disease label.

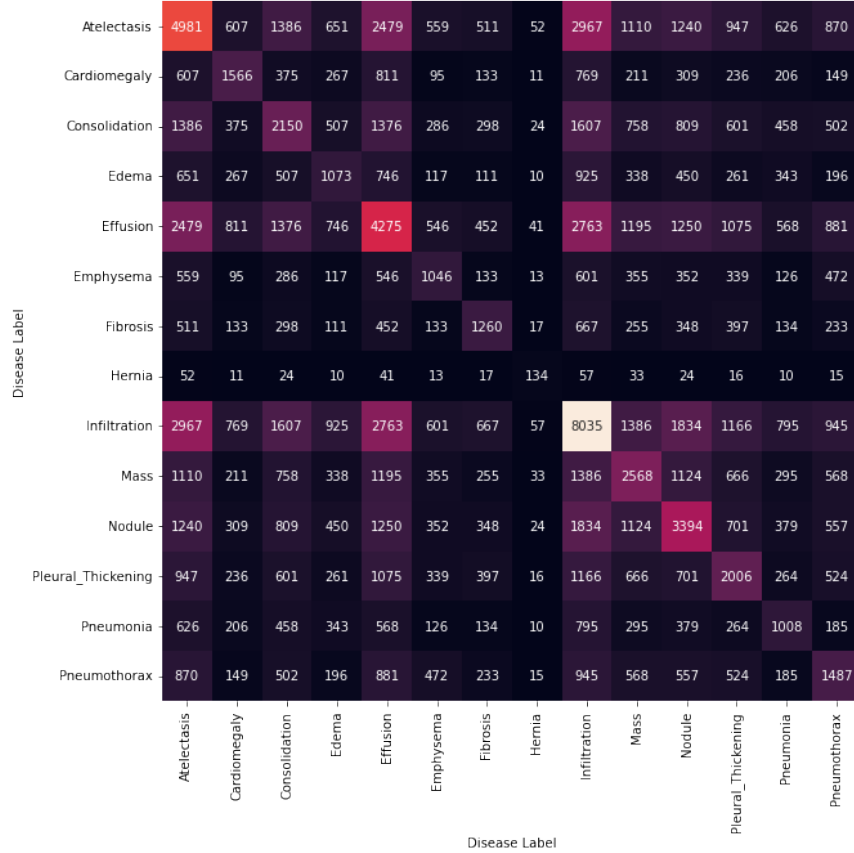


Figure 3: Co-occurrence matrix of disease labels for diagnosed patients from the NIH dataset.

Appendix B. Disease-level AUROC Scores

We have provided a detailed sub-analysis of disease-level AUROC scores, along with p-values, of the resultant surgically aggregated global models training using pairs of toy datasets, with overlapping and disjoint disease labels, sampled from the NIH dataset. The results are visualized in Appendix Tables 3 and 4.

Table 3: Disease-level AUROC scores (and p-values) on held-out NIH test set for toy datasets with overlapping disease labels. Disease labels in first dataset highlighted in blue, second dataset in green, and overlapping labels in orange.

Disease Label	Baseline	Naïve		Surgical Aggregation	
Atelectasis	0.79 (0.78, 0.80)	0.76 (0.76, 0.78)	<0.001	0.78 (0.77, 0.78)	0.01
Cardiomegaly	0.89 (0.87, 0.90)	0.89 (0.87, 0.90)	0.87	0.89 (0.87, 0.90)	0.95
Consolidation	0.81 (0.80, 0.82)	0.80 (0.78, 0.81)	0.09	0.81 (0.79, 0.82)	0.74
Edema	0.89 (0.88, 0.90)	0.87 (0.86, 0.89)	<0.001	0.89 (0.87, 0.90)	0.48
Effusion	0.87 (0.86, 0.88)	0.87 (0.86, 0.88)	0.95	0.87 (0.87, 0.88)	0.51
Emphysema	0.89 (0.88, 0.91)	0.89 (0.88, 0.91)	0.85	0.89 (0.88, 0.91)	0.78
Fibrosis	0.75 (0.72, 0.78)	0.73 (0.70, 0.76)	0.10	0.75 (0.73, 0.78)	0.80
Hernia	0.84 (0.77, 0.91)	0.86 (0.78, 0.92)	0.64	0.83 (0.74, 0.90)	0.74
Infiltration	0.69 (0.68, 0.70)	0.68 (0.67, 0.69)	0.02	0.69 (0.68, 0.70)	0.94
Mass	0.85 (0.84, 0.86)	0.85 (0.84, 0.86)	0.71	0.85 (0.83, 0.86)	0.56
Nodule	0.74 (0.72, 0.75)	0.72 (0.71, 0.74)	0.01	0.73 (0.71, 0.74)	0.07
Pleural_Thickening	0.78 (0.76, 0.79)	0.75 (0.73, 0.77)	<0.001	0.76 (0.74, 0.78)	0.08
Pneumonia	0.73 (0.70, 0.76)	0.72 (0.69, 0.74)	0.41	0.72 (0.70, 0.75)	0.74
Pneumothorax	0.87 (0.86, 0.88)	0.85 (0.84, 0.86)	0.01	0.86 (0.85, 0.87)	0.19

Table 4: Disease-level AUROC scores (and p-values) on held-out NIH test set for toy datasets with disjoint disease labels. Disease labels in first dataset highlighted in blue and second dataset in green.

Disease Label	Baseline	Naïve		Surgical Aggregation	
Atelectasis	0.79 (0.78, 0.80)	0.76 (0.76, 0.78)	<0.001	0.77 (0.76, 0.78)	<0.001
Cardiomegaly	0.89 (0.87, 0.90)	0.84 (0.83, 0.86)	<0.001	0.85 (0.83, 0.86)	<0.001
Consolidation	0.81 (0.80, 0.82)	0.80 (0.79, 0.81)	0.02	0.79 (0.78, 0.81)	0.03
Edema	0.89 (0.88, 0.90)	0.87 (0.86, 0.89)	0.01	0.88 (0.86, 0.89)	0.06
Effusion	0.87 (0.86, 0.88)	0.85 (0.86, 0.87)	<0.001	0.85 (0.84, 0.86)	<0.001
Emphysema	0.89 (0.88, 0.91)	0.85 (0.84, 0.87)	<0.001	0.87 (0.85, 0.89)	0.01
Fibrosis	0.75 (0.72, 0.78)	0.74 (0.71, 0.77)	0.36	0.75 (0.72, 0.78)	0.99
Hernia	0.84 (0.77, 0.91)	0.87 (0.80, 0.92)	0.52	0.86 (0.76, 0.92)	0.76
Infiltration	0.69 (0.68, 0.70)	0.68 (0.67, 0.69)	0.01	0.69 (0.68, 0.69)	0.28
Mass	0.85 (0.84, 0.86)	0.80 (0.80, 0.82)	<0.001	0.81 (0.80, 0.82)	<0.001
Nodule	0.74 (0.72, 0.75)	0.72 (0.70, 0.74)	0.01	0.71 (0.69, 0.72)	<0.001
Pleural_Thickening	0.78 (0.76, 0.79)	0.75 (0.73, 0.77)	<0.001	0.76 (0.74, 0.78)	0.08
Pneumonia	0.73 (0.70, 0.76)	0.71 (0.68, 0.74)	0.21	0.74 (0.70, 0.76)	0.64
Pneumothorax	0.87 (0.86, 0.88)	0.84 (0.84, 0.86)	<0.001	0.85 (0.83, 0.86)	<0.001

Appendix C. Scalability

The major shortcoming of our analysis is the lack of scalability in our experiments. Our study primarily focuses on a 2-node FL setup, which does not reflect real world FL setups where many distributed and heterogeneous nodes are involved in the training of large-scale global models. To evaluate the impact of scalability on the surgical aggregation framework, we expanded to a 14-node FL setup, where each node consisted of a subsample of the NIH dataset containing a single diagnostic task. We evaluated the surgically aggregated global model on the held-out internal NIH test set with a BCE loss of 0.24 and average AUROC of 0.71. We observed that the global model performed significantly worse than the baseline model trained on complete data ($p < 0.001$), which has a BCE loss of 0.15 and average AUROC of 0.81. We believe this significant drop in performance was the result of the observations made in Section 5. Easy-to-learn tasks overfit early in the training process and poison the distribution learned by the representation. We believe that utilizing FedBN, rather than FedAvg, to tackle imbalanced and non-iid data with domain shift, along with decaying learning rates on individual nodes, would ensure convergence of the global model (Li et al., 2019, 2021). For future work, we intend to explore both solutions in a large-scale experiment with multiple nodes that reflects a realistic FL setup.

Appendix D. Evaluation on CheXpert Validation Set

The CheXpert dataset provides a validation set ($N=200$) with ground truth determined by the consensus of three radiologist annotations, unlike the training set utilized in our analysis. In our evaluation, we evaluated the surgically aggregated and baseline models on this validation set and observed that the surgically aggregated model has excellent performance when compared to the baseline models. Since the validation set does not include any positive cases for the "fracture" label, we have dropped it from our analysis here. We observe a similar trend wherein the surgically aggregated model outperforms all baseline and naïve approaches when all observed labels are considered. The results are detailed in Appendix Table 5.

Table 5: Model metrics on CheXpert validation set ($N=200$) across (a) the 7 common labels (Fig. 1) and (b) all CheXpert labels except fracture.

(a)			(b)		
Model	CheXpert Validation		Model	CheXpert Validation	
	Loss	AUROC		Loss	AUROC
NIH Baseline	0.61	0.77 (0.74, 0.81)	NIH Baseline	-	-
CheXpert Baseline	0.37	0.83 (0.80, 0.86)	CheXpert Baseline	0.42	0.75 (0.72, 0.77)
Naïve	0.37	0.82 (0.78, 0.86)	Naïve	0.42	0.71 (0.68, 0.73)
Naïve FedAvg	0.37	0.85 (0.81, 0.88)	Naïve FedAvg	0.49	0.77 (0.74, 0.79)
Surgical Aggregation	0.36	0.85 (0.81, 0.87)	Surgical Aggregation	0.43	0.78 (0.75, 0.80)

Appendix E. Learning Intrinsic Relationships

Unlike naïve approaches considered in our work to train a model using NIH and CheXpert datasets considered, our results suggest that surgical aggregation has the ability to learn intrinsic relationships between similar but different tasks. Our results demonstrate that surgical aggregation outperforms, not just naïvely concatenating both datasets to train a model locally, but also a naïve FedAvg implementation on all observed labels. While this observation warrants an extensive analysis beyond the scope of this paper, we have included some preliminary findings for the purpose of furthering research in data harmonization.

The NIH and CheXpert datasets consist of labels that are different, but related. For example, NIH provides a label for mass while CheXpert provides a label for lesions. Since lesions larger than 3cm are considered as masses, both labels are related, but characterize different abnormalities. In another example, NIH provides a label for consolidation while CheXpert provides labels for both consolidation and lung opacity.

Using the held-out internal NIH test set, we generated sigmoid outputs for all 20 unique labels and used Youden’s J statistic to determine the optimal threshold for each disease label. In a multi-label scenario with n labels, we will have n different optimal thresholds. We utilized these thresholds to classify sigmoid outputs for each disease label as 0 or 1. Finally, we created contingency matrices for both previously mentioned examples, visualized in Appendix Fig. 4.

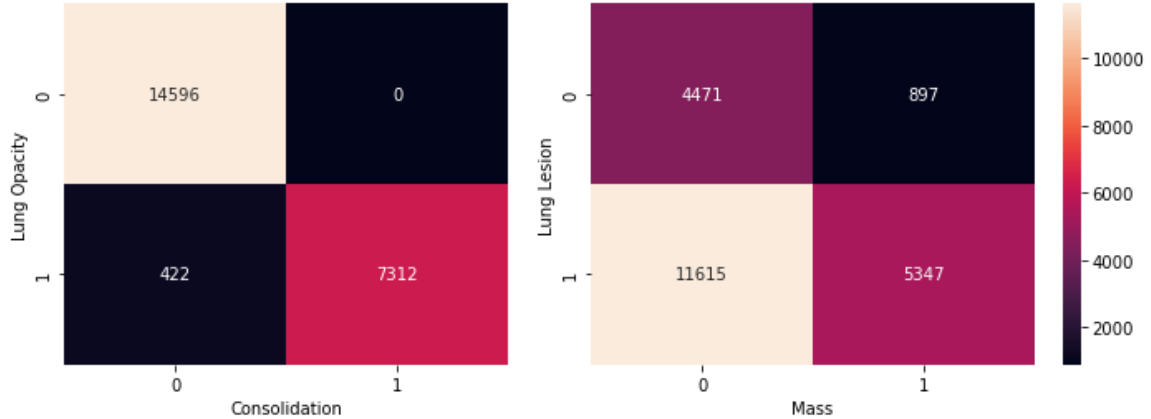


Figure 4: Contingency matrices of predictions for related labels.

These preliminary results suggest that surgical aggregation was able to form intrinsic correlations between related, but different, disease labels. In the case of masses and lesions, surgical aggregation potentially formed a clinically-useful correlation that all masses are lesions ($P(\text{lesion} = 1 | \text{mass} = 1) = 0.86$), but not all lesions are masses ($P(\text{mass} = 1 | \text{lesion} = 1) = 0.32$). Similarly, in the case of consolidation and lung opacity, we observed that the surgically aggregated model potentially formed a correlation that consolidation is a lung opacity ($P(\text{opacity} = 1 | \text{consolidation} = 1) = 1.00$). While this result is preliminary in nature, we believe these observations warrant further research and we intend to explore this extensively in our future work.